*Bangladesh Journal of Physics, Vol. **30**, Issue 1, pp. 13–22, June 2023*

SUBSTRATE TEMPERATURE DEPENDENCE OF SURFACE MORPHOLOGY AND STRUCTURE OF N-TYPE Fe_2O_3 THIN FILMS WITH ENHANCED TRANSPARENCY

MEHNAZ SHARMIN[1*], JIBAN PODDER[2] AND KHANDKER SAADAT HOSSAIN[3]

[1,2]Department of Physics, Bangladesh University of Engineering and Technology, Dhaka-1000, Bangladesh*
[3]Department of Physics, University of Dhaka, Dhaka-1000, Bangladesh

**Corresponding author e-mail: mehnaz@phy.buet.ac.bd*

Received on 06.11.2022., Revised received on 11.01.2023, Accepted for publication on 20.01.2023.

DOI: ***https://doi.org/10.3329/bjphy.v30i1.68373***

ABSTRACT

This work reports the effect of substrate temperature (T_S) on the structure, surface morphology, optical, and electrical properties of iron (III) oxide (Fe_2O_3) thin films. Fe_2O_3 thin films were deposited from the aqueous solution of ferric chloride hexahydrate at various T_S between 573 and 773 K using the spray pyrolysis technique. In field emission scanning electron and atomic force microscopic analysis, the surface of Fe_2O_3 films comprised nanoparticle clusters. In X-ray diffraction analysis, Fe_2O_3 thin films showed a rhombohedral-hexagonal structure with the predominant orientation along (104) crystallographic plane. Crystallite size reduced from 28 to 13 nm with the increase of T_S between 573 and 773 K. In UV-vis- NIR spectroscopy, the highest transmittance was found to be 76% for the film deposited at the T_S of 673 K. Band gap of the film was obtained between 2.05 - 2.09 eV. The electrical resistivity of the films ranged from 2.2×10^5 to 9.0×10^5 Ω-cm. The films contained n-type majority carriers with carrier concentration in the order of 10^{18} cm^{-3}. Fe_2O_3 thin films with wide band gap, high transparency, and n-type conductivity indicate that the films are suitable for Fe_2O_3 in optoelectronic applications.

Keywords: *α-Fe_2O_3 thin film, Substrate temperature, XRD, FESEM, AFM.*

1. INTRODUCTION

Iron, a remarkable transition metal can form various oxide phases with different stoichiometry and crystal structures [1]. Among many phases of iron(III) oxide (Fe_2O_3), hematite or α-Fe_2O_3 is very popular because of its availability, environment-friendly properties, lower cost, and thermal and chemical stability at ambient temperature [2-4]. It exhibits n-type semiconducting nature with a rhombohedral-hexagonal crystal structure having an optical band gap of 2.2 eV [1, 2, 4, 5]. α-Fe_2O_3 has attractive properties which make it usable in several optoelectronic and environment safety applications such as gas and vapor sensors, recording media, lithium-ion batteries, supercapacitors, solar cells, solar filters, antibacterial coating, production of hydrogen, etc. [2-7]. Thin films of α-Fe_2O_3 are synthesized by several chemical reaction-based synthesis techniques like spray pyrolysis technique (SPT) [2], sol-gel [5], successive ionic layer adsorption and reaction method [7], chemical vapor deposition [8], etc. SPT is an easy and low-cost solution-based deposition technique for the synthesis of thin films with consistent chemical composition and microstructure. Several deposition parameters influence the film formation in SPT, such as

precursor material, solvent concentration, the pressure of carrier gas, spray rate, droplet size, substrate temperature (T_S), nozzle to substrate distance, etc. The structure and morphology of an SPT-deposited thin film are very much dependent on these deposition parameters. Among various deposition parameters, T_S is an important one since growth kinetics during film deposition greatly relies on the temperature at which pyrolytic decomposition occurs and it affects the structure and morphology of an SPT-deposited film. The influence of T_S on the structure and various properties of α-Fe_2O_3 thin films have been reported in some literature [2, 9-12]. Akl [2] reported the variation of structural and optical properties of α-Fe_2O_3 thin films prepared by SPT from an aqueous solution of $Fe(NO_3)_3.9H_2O$ at various T_S. Duret and Graltzel [9] published that the surface of α-Fe_2O_3 thin film prepared by ultrasonic SPT contained mesoscopic leaflet structures and that of SPT deposited α-Fe_2O_3 thin film consisted of particles. Yadav et al. [10] prepared α-Fe_2O_3 thin films by SPT from 0.25 M non-aqueous solution of $FeCl_3$ and studied structural, morphological, electrochemical, and optical properties of the films deposited at various T_S between 300 and 400 °C. Ma and Kim et al. [11] reported the effect of T_S on the structural and electrical properties of ultrasonic SPT deposited α-Fe_2O_3 thin films from iron acetylacetonate precursor in the range of T_S from 200 to 400 °C. Mishjil et al. [12] published their work on structural and topological properties of α-Fe_2O_3 thin films prepared by SPT at the T_S of 400, 450 and 500 °C. Although the effect of T_S on the structure and properties of α-Fe_2O_3 thin films have been studied by some researchers, still there is scope to investigate T_S-dependent properties of Fe_2O_3 thin films synthesized by SPT. In this work, structural, surface morphological, topological, optical, and electrical properties of Fe_2O_3 thin films synthesized at various T_S are investigated. The prime objectives of this work are to connect the results obtained from various characterization and to figure out the effect of T_S on the structure, morphology, and properties of Fe_2O_3 thin films, and to explore the suitable scope of application of the material in device fabrication.

2. MATERIALS AND METHODS

2.1 Thin film synthesis

First, the glass substrates were cleaned with ethanol and distilled water using an ultrasonic bath and air-dried in a clean environment. 0.1 M aqueous solution of iron (III) chloride hexahydrate ($FeCl_3.6H_2O$, purity 99 % MERCK, Germany) was prepared by dissolving the precursor salt in distilled water. The mixture was stirred with a magnetic stirrer for 60 min to ensure the homogeneity of the solution. A few drops of ethanol were added to the precursor solution to confirm better crystallinity. The solution was filtered and transferred into a clean beaker. A low-cost and user-friendly spray pyrolysis deposition unit was used for the preparation of Fe_2O_3 thin films. An ebonite spray gun with an outlet aperture diameter of 0.001 m was used. The following deposition parameters were kept constant during the spray process:

- The nozzle to substrate separation: 25 cm
- Air pressure: 0.50 bar
- Spray rate: 1 mL/min
- Deposition time: 10 min

The films were deposited at various T_S from 573 - 773 K in the step of 50 K. The T_S was measured by a Copper- Constantan thermocouple during deposition.

2.2 Characterization techniques

The surface morphology of the deposited films was investigated using a field emission scanning electron microscope (FESEM) (JEOL JSM-7600F, Japan). FESEM images were captured at 30000 (30k) magnification. The ImageJ version 2018 software was used for analyzing the average particle size from the FESEM images. The complete area of the FESEM images was considered while determining the average particle size. A set of particle size distribution data were obtained from the ImageJ software. Then the data was plotted as histograms and statistically analyzed via Gaussian fit of graphs. Topographical analysis of the thin films was performed using a Nanosurf FlexAFM (Switzerland) atomic force microscope (AFM). The average roughness (R_a) and root-mean-square roughness (R_q) of the film surface were measured from the AFM image with SPM control software version 3.1. Structural analysis of the films was performed by an X-ray powder diffractometer (PANalytical EMPYREAN SERIES 2, Netherlands) using X-rays of wavelength 1.5406 Å from CuK_α target operated at an input power of 60 kV. "X'Pert Highscore" computer software was used to study 2θ values, interplanar spacing (d) value, and full width at half maximum (FWHM). The structural parameters were compared with the standard data of α-Fe_2O_3 (JCPDS card: 24-0072). Measurement of film thickness was done by the Fizeau fringe method [13]. The optical transmission spectra of the films were recorded at room temperature using a dual beam UV-Vis-NIR spectrophotometer (Dynamica Halo DB-20, Australia) in the spectral range of 200-1100 nm. Hall Effect measurement of the films was done by a Hall Effect measuring apparatus (ECOPIA HMS-5000, USA) applying the magnetic field 0.54 T and current 10 mA at room temperature (300 K).

3. RESULTS AND DISCUSSION

3.1 Surface morphology

The surface morphology of Fe_2O_3 thin films prepared at various T_S is presented by the FESEM images in Fig. 1. The FESEM images of Fe_2O_3 thin films show that the thin films contain nanoparticle clusters. The surface of the films deposited at T_S 673, 723, and 773 K show rough morphological features. The formation of rough morphological features may be related to the fact that the growth kinetics of film is ruled by pyrolytic decomposition in the vapor state of spray solution at elevated T_S [14]. During the preparation of thin films by SPT at lower T_S, a spray droplet decomposes in the liquid phase after being splashed onto the heated substrate [14]. That is why nanoparticles are not clearly visible in Fig. 1 (a). With the increase of T_S complete decomposition of the spray droplet occurs during the flight and dry precipitate is deposited onto the substrate [14]. Fig. 1 (b) represents a dry decomposed pattern of the nanoparticle agglomerates. When T_S is increased even more the dry nanoparticle precipitate created in the vapor form is decomposed and diffused to the substrate [14]. The result of decomposed deposition of dry precipitate is visible in Fig. 1 (c). At very high T_S the spray droplet is completely vaporized and dissociated into nanoparticles, which are deposited onto the substrate giving rise to a very rough aspect [14]. An increase in surface roughness with the increase of T_S has been reported for Fe_2O_3 thin films by other workers [10, 12]. Particle size distributions of as-deposited Fe_2O_3 thin films are shown in the histograms of Fig. 1 and the average particle size is calculated from the Gaussian fit of the histograms. The average particle size decreases between 57.5 and 35 nm with the rise of T_S. The randomness of the particle size distribution is more in the films synthesized at the higher T_S.

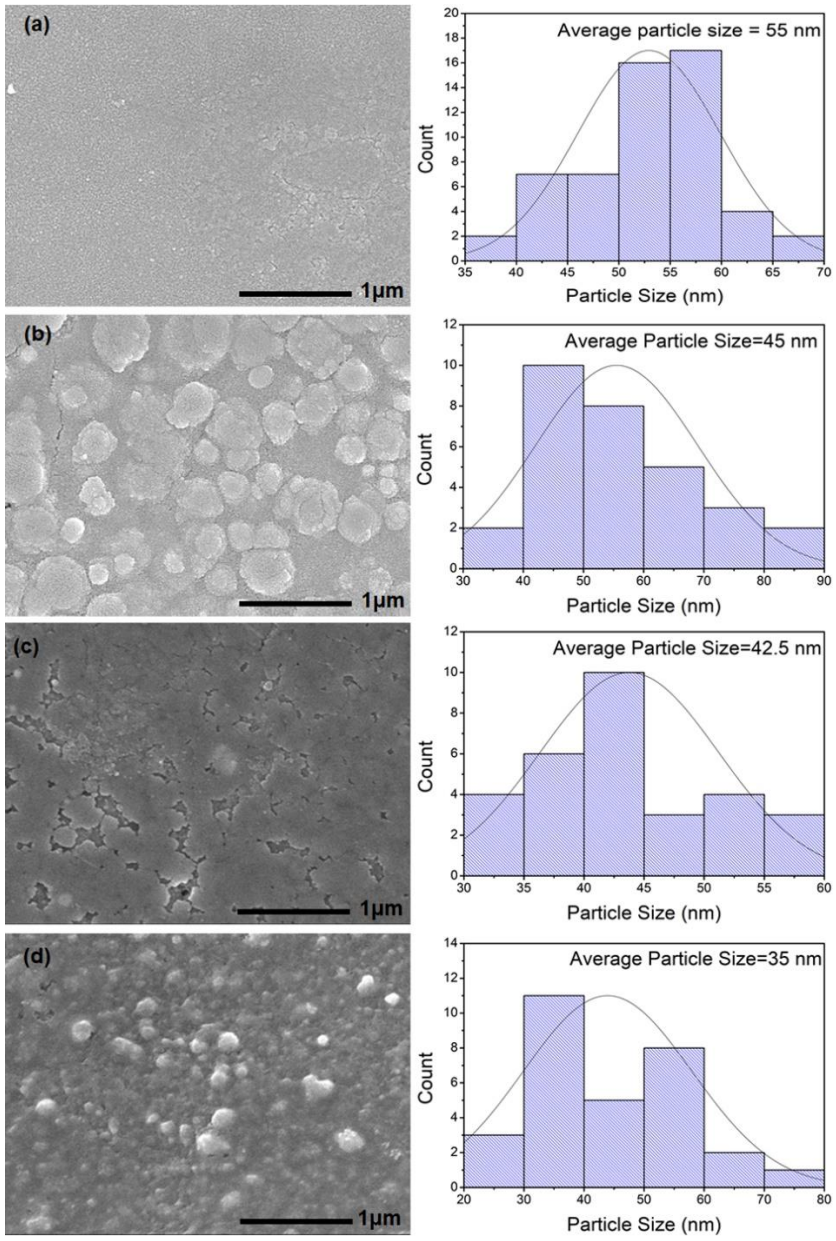

Fig. 1 FESEM images of Fe_2O_3 thin films deposited at the T_S of (a) 623, (b) 673, (c) 723 and (d) 773 K the histograms for determination of average particle size

3.2 Structural analysis

XRD patterns of Fe_2O_3 thin films are shown in Fig. 2. The XRD patterns were compared with the standard data (JCPDS card no. 24-0072 for α-Fe_2O_3 and JCPDS card no. 39-1346 for γ-Fe_2O_3).

Fe_2O_3 thin film prepared at the T_S of 573 K exhibits two less intense peaks along (202) and (104) orientations. The (202) peak corresponds to the γ-Fe_2O_3 structure and the (104) corresponds to the α-Fe_2O_3 structure. It can be said that this film has poor crystallinity and is a mixture of α-Fe_2O_3 and γ- α-Fe_2O_3 phases. The characteristic peaks corresponding to rhombohedral hexagonal structure or the α-Fe_2O_3 are found in the films prepared at the T_S of 623, 673, and 773 K. In the XRD patterns of the films prepared at 623, 673, and 773 K, (104) is the predominant peak. There was no peak corresponding to γ-Fe_2O_3. The position of (104) peak in the standard data of the α-Fe_2O_3 is 33.115°. The (104) peak position is shifted towards the right for the film prepared at 623 K and for the films prepared at 673 and 773 K the peak shifts towards the left with respect to the standard data. It indicates the change in reaction mechanism during film formation with the increase of T_S. At 623 K the reaction on the surface of the substrate occurs in the liquid phase giving rise to a compact and flawless deposition as found in Fig.1. Whereas at 673 and 773 K dry decomposition of the spray solution causes the formation of randomly orientated of particle agglomerates on the substrate surface Fig.2. The differences in surface morphology cause the shifting of the preferential (104) orientation of the film. An analogous variation of the crystalline nature of α-Fe_2O_3 thin films with the increase of T_S is observed in some other papers [2, 11].

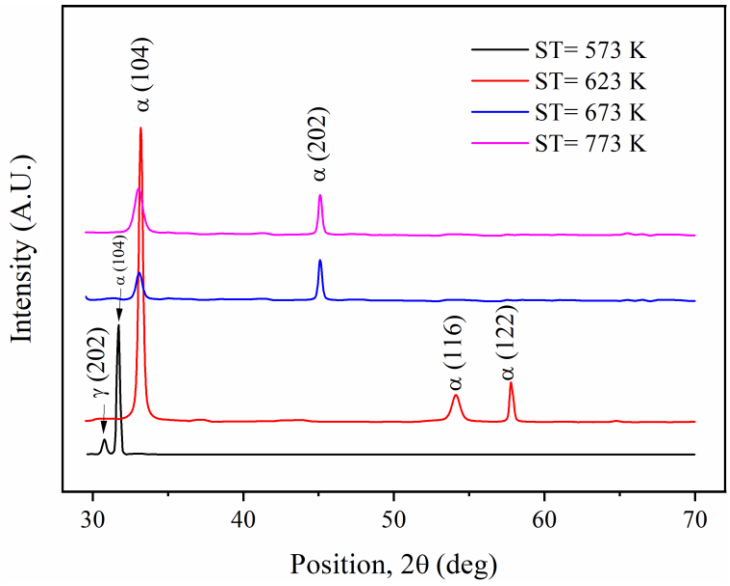

Fig. 2 XRD patterns of Fe_2O_3 thin films deposited at the various T_S

Crystallite size (D) and dislocation density (δ) of Fe_2O_3 thin films is calculated by the Scherrer formula [15] and Williamson-Smallman's formula [16] presented in equations (1) and (2). The strain (ε) of Fe_2O_3 thin films is calculated using the relations given in equation (3) [17].

$$D = \frac{K\lambda}{\beta \cos\theta} \quad (1)$$

$$\delta = \frac{1}{D^2} \quad (2)$$

$$\varepsilon = \frac{\beta \cos\theta}{4} \quad (3)$$

Structural parameters of Fe_2O_3 thin films are enlisted in Table. 1. It is seen that the D of Fe_2O_3 thin films decrease, whereas ε and δ increase with the rise of T_S. The decrease of D with the increase of T_S may be attributed to the effect of change, of growth mechanism via an increase of the amount of chemical decomposition in the vapor phase giving rise to the formation of smaller nanoparticle agglomerates [14]. The increasing tendency of ε and δ of Fe_2O_3 films is an indication of the increase of deformation in the size of particles and dislocations in the whole structure.

Table. 1 Structural parameter calculated for Fe_2O_3 thin films

T_S (K)	D (nm)	$\varepsilon \times 10^{-3}$	$\delta \times 10^{-3}$ (nm^{-2})
573	28	1.24	1.28
623	27	1.28	1.37
673	18	1.98	3.09
773	13	2.60	5.92

3.3 Topographical analysis

AFM images of Fe_2O_3 thin films are taken in the scanned area 10.3 μm × 10.3 μm and the films show distributions of particle agglomerates and pores on the surface. Fig. 3 display that there are peaks and valleys on the surface of the films. Fig. 3 (a), (b), (c), and (d) show the AFM images of the Fe_2O_3 thin films prepared at the T_S of 573, 623, 723, and 773 K, respectively. The film prepared at 623 K seem to be more porous than that prepared at 773 K. It is in good agreement with the FESEM images in Fig. 1.

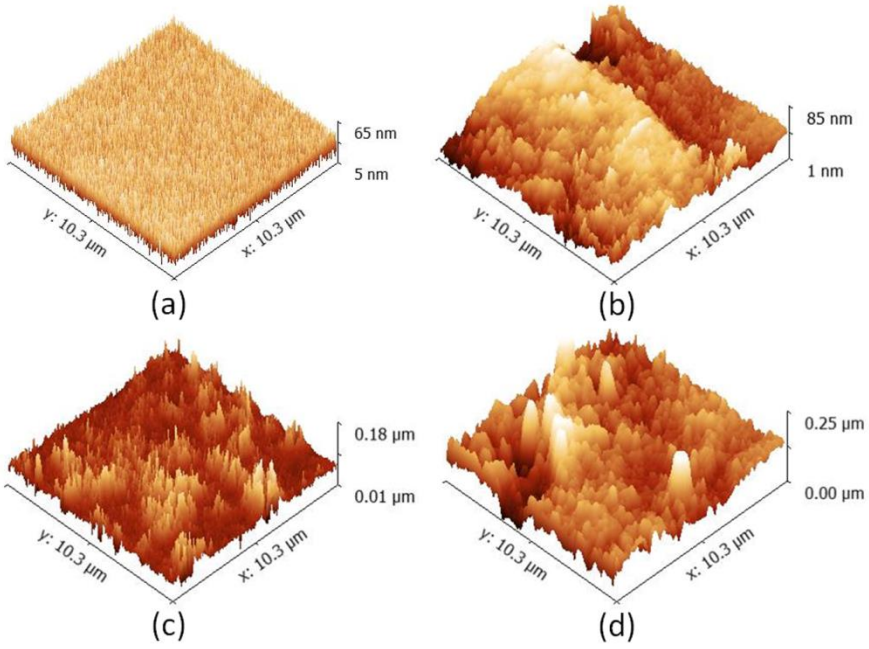

Fig. 3 AFM images of Fe_2O_3 thin films deposited at the T_S of (a) 573, (b) 623, (c) 723 and (b) 773 K

The R_a and R_q of Fe_2O_3 thin films are exhibited in Table. 2. The numerical values of R_a and R_q designate the increment of the roughness of Fe_2O_3 thin films with T_S. The results of the AFM analysis are consistent with the results of the FESEM analysis.

Table. 2 Roughness analysis of Fe_2O_3 thin films.

T_S (K)	R_a (nm)	R_q (nm)
573	7.81	9.56
623	13.78	16.50
723	21.67	29.68
773	27.93	41.33

3.4 Optical properties

Transmission spectra of Fe_2O_3 thin films deposited at the various T_S are plotted in Fig. 4. The films are found transparent in the visible-near infrared (vis-NIR) region. In Fig. 4, there is a slight increase of transmittance (T%) with the increase of T_S in the range 573 - 723 K and then it reduces for the film prepared at the T_S of 773 K. The highest T% is 76%, obtained for Fe_2O_3 thin film synthesized at T_S of 673 K. An increase of T% with T_S may be attributed to the decrease of the D value of the film and surface morphological changes as shown in Table. 1 and Fig. 1, respectively. Despite having less D value T% of the Fe_2O_3 thin film deposited at 773 K is less, which may occur due to the very high surface roughness of the film as found in FESEM image Fig. 1 and roughness analysis in Table. 2.

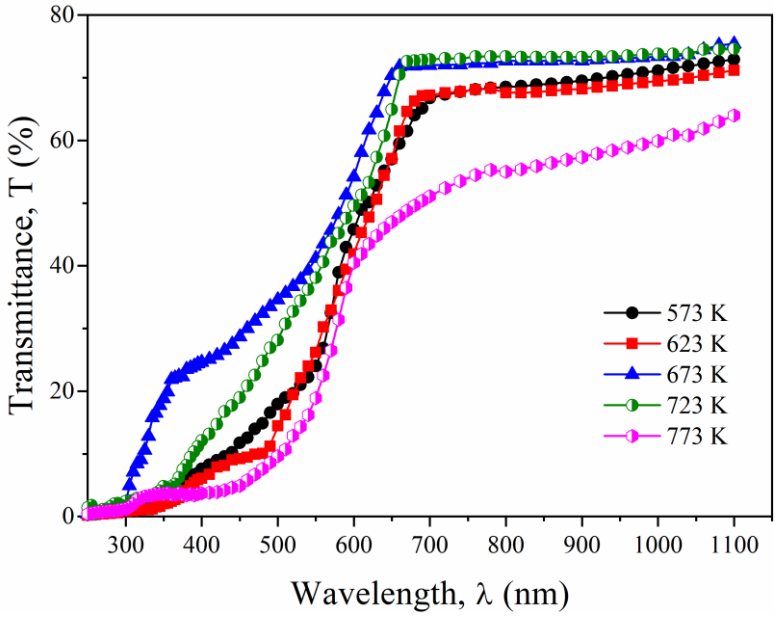

Fig. 4 Transmission spectra of Fe_2O_3 thin films deposited at the various T_S

The extinction coefficient (k) of Fe_2O_3 is calculated using the formulae, $k = \alpha\lambda/4\pi$ [18] and exhibited in the Table. 3. The optical band gap (E_g) is computed using the Tauc equation, $\alpha h\nu = B\,(h\nu - E_{opt})^n$ [19]. Refractive index (η) is calculated using the equation, $\eta = (1+R)/(1-R) + \sqrt{\{4R/(1-R)^2\} - k^2}$ [20]. E_g of Fe_2O_3 thin films is estimated from the Tauc plots presented in Fig. 5. E_g reduces very slightly in the range 2.09 – 2.05 eV with the increase of T_S. So, it can be said that T_S has no remarkable effect on the E_g of Fe_2O_3 thin films. E_g values are in good agreement with the standard value for Fe_2O_3 (2.20 eV) and values reported by other workers [2, 10].

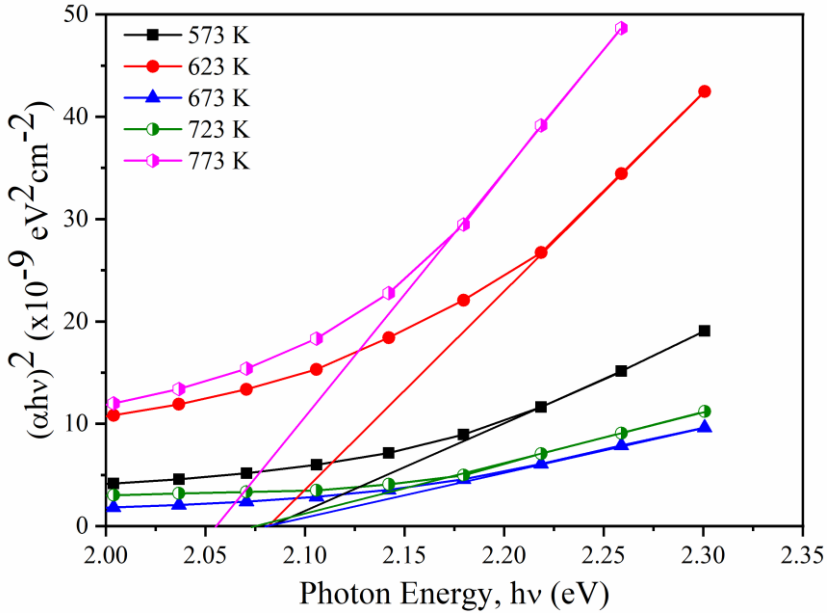

Fig. 5 Tauc plots Fe_2O_3 thin films deposited at the various T_S

Table. 3 Optical properties of Fe_2O_3 thin films deposited at the various T_S.

T_S (K)	E_g (eV)	η (at 650 nm)	k (at 650 nm)
573	2.09	2.35	0.25
623	2.08	2.31	0.24
673	2.08	2.24	0.14
723	2.07	2.23	0.13
773	2.05	2.47	0.29

In Table. 3, η and k values decrease a little with the rise of T_S up to 723 K indicating the reduction of optical density of the medium and the less absorbing nature of the Fe_2O_3 films. Fe_2O_3 thin film prepared at 773 K shows higher η and k values than others. It indicates the presence of highly disordered states in the Fe_2O_3 films prepared at the T_S of 773 K due to high surface roughness.

3.5 Electrical transport properties

Electrical resistivity (ρ), carrier concentration (n), Hall mobility (μ), and Hall coefficient (R_H) Fe_2O_3 thin films are shown in Table. 4. ρ, μ and R_H values of Fe_2O_3 thin films reduce for the film deposited between the T_S 573 and 673 K and increase for the films synthesized at the T_S above 673 K. ρ is found to be in the order of 10^5 Ω-cm which match with that found by other workers [21]. The negative value of R_H indicated that Fe_2O_3 thin films contains n-type majority carriers. All these electrical properties are dependent on the number of charge carriers in the film. The order of n is found 10^{18} cm^{-3} in the Fe_2O_3 thin films, the order matches nicely with some earlier published papers [23, 24]. n increases with T_S up to 673 K and then it reduces slightly. The maximum value of n is found in Fe_2O_3 thin film deposited at 673 K indicating the availability of carriers to participate in transport. Increase and decrease of n, μ and R_H occur due to the carrier scattering mechanism associated with the native defects. Although there is no specific pattern of variation in ρ, μ, R_H and n, it is still evident that all the films have n-type carriers with high mobility.

Table. 4 Electrical properties of Fe_2O_3 thin films deposited at the various T_S

T_S (°C)	ρ (× 10^5 Ω-cm)	μ ($cm^2V^{-1}s^{-1}$)	R_H (cm^3C^{-1})	n (× 10^{18} cm^{-3})
300	4.1	7.6	-3.11	2.01
350	2.2	6.6	-1.43	4.38
400	3.0	3.8	-1.13	5.54
450	8.6	3.7	-3.20	1.95
500	9.0	5.6	-3.34	1.87

4. CONCLUSIONS

Structural, morphological, topographical, optical, and electrical properties of Fe_2O_3 thin films synthesized at various T_S in the range of 573 – 773 K are thoroughly studied in this work. The surface morphology of the films is found to be significantly influenced by the difference in growth mechanism at various T_S. Fe_2O_3 deposited at 573 K shows weak crystallinity with the mixture of α and γ phases of Fe_2O_3, whereas the films prepared above 573 K T_S exhibits only α-Fe_2O_3 phase with the preferential orientation along the (104) plane. Crystallite size was reduced from 28 to 13 nm with T_S. Higher roughness values are found for the Fe_2O_3 film prepared at 773 K. Fe_2O_3 thin films were transparent in the vis-NIR region of light. Optical band gap, refractive index, and extinction coefficient of Fe_2O_3 thin films show a little reduction with T_S up to 673 K. Reduced transmittance, high extinction coefficient, and high refractive index is obtained in the Fe_2O_3 film deposited at 773 K because of its high surface roughness. Electrical parameters like resistivity, carrier mobility, Hall coefficient, and carrier concentration of Fe_2O_3 thin films show irregular variations due to the existence of native defects. The high n-type carrier concentration of Fe_2O_3 thin films indicated the availability of charge carriers to participate in transport. Transparent and crystalline Fe_2O_3 thin films having high band gap, refractive index, n-type carrier concentration, and carrier mobility can be produced at the T_S between 573 and 673 K. It is likely that Fe_2O_3 thin films grown in favorable T_S can be used for optoelectronic devices.

ACKNOWLEDGMENTS

The authors are grateful to the authority of BUET for financial support and Material Science Division, Atomic energy Center, Dhaka, Bangladesh, for providing necessary laboratory support for Hall effect measurement. The author (Mehnaz Sharmin) is thankful to Bangabandhu Science and Technology Fellowship Trust for awarding her Ph. D. Fellowship for the financial year 2017-2018. One of the authors gratefully acknowledges support from International Science Program (ISP), Uppsala University, Sweden.

REFERENCES

1. R. M. Cornell and U. Schwertmann, Iron Oxides: Structure, Properties, Reactions, Occurrences and Uses (New York: Wiley-VCH Verlag GmbH & Co. KGaA Weinheim), Ch-10, p-121 (2003).
2. A. Akl , Appl. Surf. Sci. **233** (2004) 307.
3. Q. Wei, Z. Li, Z. Zhang and Q. Zhou, Mater. Trans. **50** (2009) 1351.
4. J. Wu, Y. Lee, H. Chiang and D. Wong, J. Phys. Chem. B **110** (2006) 18108.
5. L. Armelao, G. Granozzi, E. Tondello, P. Colombo, G. Principi, P. P. Lottici and G. J. Antonioli, J. Non-Cryst. Solids **192-193** (1995) 435. A. U. Ubale and M. R. Belkhedkar, J. Mater Sci Technol. **31** (2015) 1.
6. M. R. Belkhedkar and A. U. Ubale, J. Mater. Chem. **4** (2014) 109.
7. T. Maruyama and T. Kanagawa, J. Electrochem. Soc. **143** (1996) 1675.
8. A. Duret and M. Graltzel, J. Phys. Chem. B **109** (2005) 17184.
9. A. A. Yadav, T. B. Deshmukh, R. V. Deshmukh, D. D. Patil and U. J. Chavan, Thin Solid Films **616** (2016) 351.
10. T. Y. Ma and J. G. Kim, J. Sensors Soc. **13** (2004) 127.
11. K. A. Mishjil, A. A. Kamil and A. N. Jasim, Diyala J. Pure Sci. **11** (2015) 1.
12. S. Tolansky, Multiple Beam Interferometry of Surfaces and Films (London: Oxford Clarendon Press, 1948).
13. D. Perednis and L. J. Gauckler, J. Electroceramics **14** (2005) 103.
14. P. Scherrer, Nachr Ges Wiss Goettingen Math-Phys Kl **1918** (1918) 98.
15. G. K. Williamson and R. E. Smallman, Philos. Mag. **1** (1956) 34.
16. Y. Zhao and J. Zhang, J. Appl. Crystallogr. **41** (2008) 1095.
17. R. E. Hummel Electronic Properties of Materials (New York: Springer-Verlag) (2000).
18. E. A. Davies and N. F. Mott, Philos. Mag. **22** (1970).
19. W. D. Callister Jr. Fundamentals of Materials Science and Engineering, (New York: John Wiley & Sons, 2001).
20. R. A. Ismail, Y. Najim and M. Ouda, e-J. Surf. Sci. Nanotech. **6** (2008) 96.
21. S. Mohanty and J. Ghose, J. Phys. Chem. Solids. **53** (1992) 81.
22. J. E. Turner, M. Hendewerk, J. Parmeter, D. Neiman and G. A. Somorjai, J. Electrochem. Sac. **131** 1777 (1984).